

## Article

# Systematic Calculation of Yield and Failure Curvatures of Reinforced Concrete Cross-Sections

John Bellos <sup>1,\*</sup>  and Apostolos Konstantinidis <sup>2</sup><sup>1</sup> Department of Civil Engineering, Neapolis University Pafos, Paphos 8042, Cyprus<sup>2</sup> BuildingHow PC, 11635 Athens, Greece; apl@pi.gr

\* Correspondence: j.bellos@nup.ac.cy

**Abstract:** This paper examines and provides a robust solution to the problem of yield and failure curvatures of reinforced concrete (RC) cross-sections, taking into account cracking. At the same time, it calculates the corresponding necessary reinforcement or the moment of resistance in both yield and failure limit states. Computationally, the problem of determining the actual curvatures is reduced to the bending design problem of the cross-section in the yield and failure limit states. This study shows the researcher and the designer how to systematically calculate the strains for different concrete and steel grades and for standard or random cross-sections. This complex process is quite necessary to determine the respective curvatures. The main concept is presented with an emphasis on the “solution regions” as well as the critical cases of the “asymptotic regions”, both in yield and failure limit states. Our wide-ranging research on RC element design under biaxial bending with axial force for both yield and failure limit states has been completed and validated via sophisticated algorithms and is available for publication.

**Keywords:** curvature; ductility; yield; failure; moment of resistance; reinforcement; bending; design



**Citation:** Bellos, J.; Konstantinidis, A. Systematic Calculation of Yield and Failure Curvatures of Reinforced Concrete Cross-Sections. *Buildings* **2024**, *14*, 826. <https://doi.org/10.3390/buildings14030826>

Academic Editors: Duc-Kien Thai, Atsushi Suzuki and Dinil Pushpalal

Received: 8 January 2024

Revised: 1 March 2024

Accepted: 14 March 2024

Published: 19 March 2024



**Copyright:** © 2024 by the authors. Licensee MDPI, Basel, Switzerland. This article is an open access article distributed under the terms and conditions of the Creative Commons Attribution (CC BY) license (<https://creativecommons.org/licenses/by/4.0/>).

## 1. Introduction

The yield and failure curvatures, as well as the respective stiffnesses, depend on cross-section geometry, the amount and distribution of reinforcement, the reinforcement material properties, the concrete material properties, and the axial forces. The large relative displacements of the column heads in relation to their bases, and therefore those displacements of the associated diaphragms, significantly increase the characteristic periods of the building, thus resulting in low seismic accelerations. This fact is very important for the structural robustness of the building, especially when checking the resistance of an existing building structure to an earthquake.

Many researchers dealt with the specific problem in the past. Chen and Hsu [1] developed a semi-empirical formula for the curvature ductility of doubly reinforced beam sections, which, via performance-based design, takes into account the effect of reinforcement ratios as well as the reinforcement and concrete strengths. Hernández-Montes et al. [2] related the curvature ductility capacity of cross-sections designed with optimal reinforcement to those with symmetric reinforcement, for both unconfined and confined concrete cases, under varying axial loads, gross section area, and concrete strength. Chandrasekaran et al. [3] developed a closed form solution to estimate the curvature ductility of RC elements under service loads, considering the nonlinear characteristics of constitutive materials and the reinforcement ratios as required by Eurocodes. Arslan and Cihanli [4] produced a formula predicting the curvature ductility of reinforced high-strength concrete beams based on the parametric study of experimental results to evaluate the effects of various structural parameters. Lee [5] provided a prediction formula for the curvature ductility factor of doubly reinforced beam sections, taking into account the concrete strength, the tensile yield strength of steel, and the compressive ultimate strength of steel. Laterza et al. [6] performed an efficiency study of codal detailing rules for reinforcement

design of primary columns and beams within the critical regions by comparing the codal design results to the measured curvature ductility. By examining the effects of spectral acceleration and a strong column factor, Zhou et al. [7] provided an empirical model in the form of a quantitative relationship between the curvature ductility demands of columns and the global displacement ductility demands of frame structures. Baji and Ronagh [8] developed a probabilistic method used to calculate curvature ductility by means of the central limit theorem, considering the specific behavior of the moment redistribution factor with respect to curvature ductility and plastic hinge length. Research on biaxial bending by Breccolotti et al. [9] produced a formula for the curvature ductility of reinforced short columns of varying section geometry, neutral axis direction, reinforcement ratios, and axial forces. Kollerathu [10] proposed an equation to evaluate and compare the curvature ductilities of reinforced masonry and RC walls, as a result of diagrams of flexural strength versus curvature. Recently, Foroughi and Yuksel [11] developed a predictive formula for the curvature ductility of doubly-reinforced beams by performing a numerical parametric study.

Finding the actual curvatures, both in yield and failure states, requires the calculation of concrete strain and steel strain under axial force and bending moment (or equivalently, reinforcement), an extremely complex computational problem with a wide range of solutions. Calculation tables were also used in the past, but they were available in failure states only and usually for specific materials. Nowadays, due to the variety of available materials and the demand for checking the actual strength and possibly retrofitting existing buildings, the design in limit states also becomes imperative. This is the reason for our extensive research to find a robust theoretical solution to the bending design problem, both in yield and failure limit states, a part of which is presented in this article.

## 2. Column Limit States

### 2.1. Column in Yield Limit State

Figure 1 presents an exaggerated model of a column in the yield limit state. Flexural cracks are perpendicular to the axis of the bar, while shear cracks have an inclination of  $45^\circ$  to  $60^\circ$  to the axis of the bar. Here,  $\delta_1$  is the displacement due to shear, which is linear and does not affect the curvature, and  $\delta_2$  is the displacement due to crack causing bending at the yield limit state.

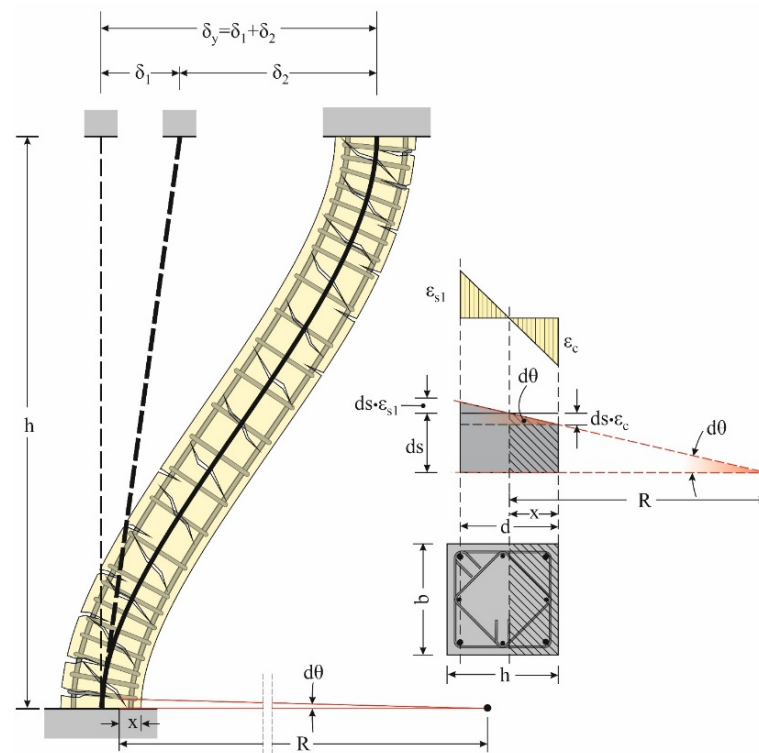


Figure 1. Column in yield limit state (not to scale).

Considering a differential length  $ds$  of the column at the side of its cross-section, the inner fiber compresses and shortens by  $ds \cdot \varepsilon_c$ , while the outer fiber stretches and expands by  $ds \cdot \varepsilon_{s1}$ . Then, the resulted differential central angle  $d\theta$  is as follows:

$$d\theta = ds \cdot (\varepsilon_c + \varepsilon_{s1}) / d \text{ and } d\theta = ds / R \quad (1)$$

Equation (1) yields the following:

$$ds / R = ds \cdot (\varepsilon_c + \varepsilon_{s1}) / d \rightarrow \varphi_y = 1 / R = (\varepsilon_c + \varepsilon_{s1}) / d \quad (2)$$

where  $\varphi_y$  represents the actual yield curvature [12].

Note that in the yield state, it must be  $\varepsilon_c \leq \varepsilon_{c2}$  and  $\varepsilon_{s1} \leq \varepsilon_{yd}$ , where the yield strain for at least one of the two materials, either  $\varepsilon_c$  of the concrete or  $\varepsilon_{s1}$  of the steel, has been reached.

## 2.2. Column in the Failure Limit State

The physical behavior of a column functioning in a failure limit state is represented in Figure 2 through the only possible observational method, which is the experimental one. The experiment, which was part of the “Anti-Seismic Thoraces” tests, took place in 1998 in the NTUA’s Reinforced Concrete Laboratory under the auspices of Professor Theodosios Tassios. It is evident that the column failure takes place in relatively small regions at the ends, while the rest of the column is in a yield state (marginal yielding with cracking) [12,13].

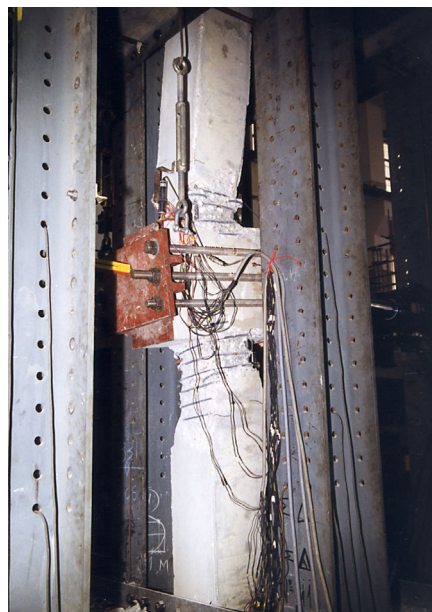


**Figure 2.** The way to create a plastic joint at the two ends of a node due to strong alternating tension (Tests of “Anti-Seismic Thoraces”—Reinforced Concrete Laboratory, NTUA).

Figure 3 presents an exaggerated model of a column in the failure limit state. Flexural and shear cracks are apparent at the critical end regions of the column, while along the rest of the body, they remain similar to the yield limit state case.

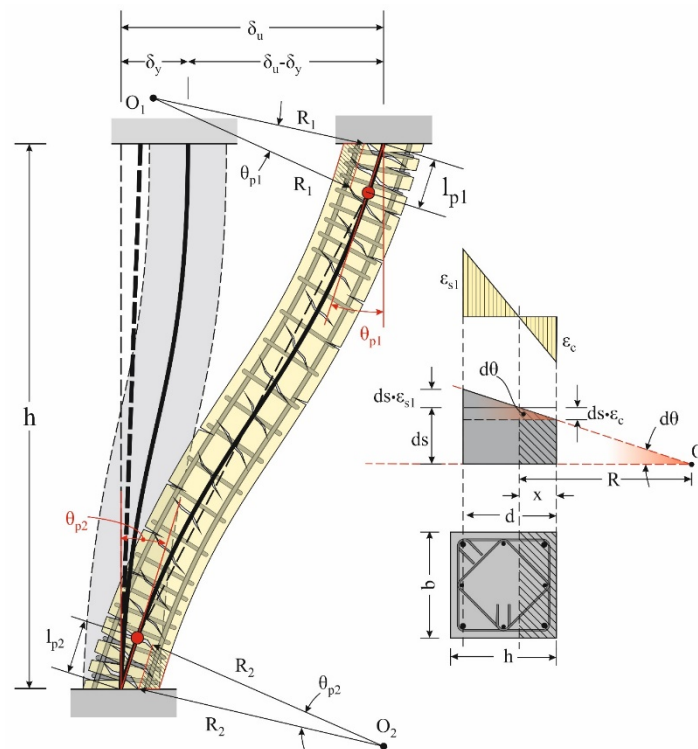


Figure 3. Column in the failure limit state with plastic joints at both ends (not to scale).

The failure curvatures  $\varphi_u$  are calculated in exactly the same way as the yield limit state, as follows:

$$\varphi_{u,j} = 1/R_j = (\epsilon_c + \epsilon_{s1})/d, \quad j = 1, 2 \quad (1 = \text{head}, 2 = \text{base}) \quad (3)$$

When the reinforcement of the head and base is the same, as is generally the case, then  $\varphi_{u,1} = \varphi_{u,2} = \varphi_u$ . Note again that in the failure state, it must be  $\epsilon_c \leq \epsilon_{cu2}$  and  $\epsilon_{s1} \leq \epsilon_{ud}$ , where the failure strain of at least one of the two materials, either  $\epsilon_c$  of the concrete or  $\epsilon_{s1}$  of the steel, has been reached.

### 2.3. Example: Calculation of Limit State Curvatures

Let us consider a fixed–fixed support column of height  $h = 3.0$  m under axial force  $N_d = -800$  kN (see Figure 1). The cross-section is  $400 \text{ mm} \times 400 \text{ mm}$ ,  $f_{ck} = 30 \text{ MPa}$ ,  $\gamma_c = 1.50$ ,  $f_{yk} = 500 \text{ MPa}$ ,  $\gamma_s = 1.15$ ,  $\epsilon_{su} = 20\%$ , and  $K = 1.0$  with  $d_1 = d_2 = 50 \text{ mm}$ . The applied reinforcement is  $4\Phi 20 + 4\Phi 14$  ( $=1860 \text{ mm}^2$ ,  $\rho = 1.16\%$ ). It is considered that 50% of the total reinforcements are placed at the corners, while the rest are distributed along the sides (see Figure 4).

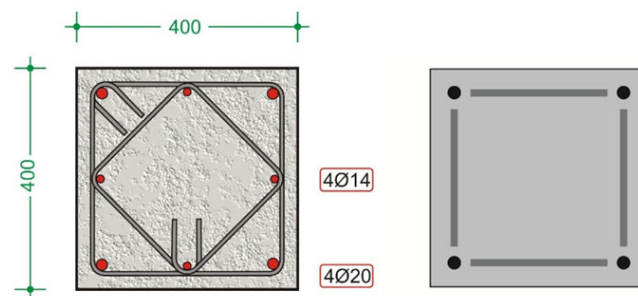


Figure 4. Column cross-section with its reinforcement and corresponding model for bending design.

Required: the yield curvatures  $\varphi = 1/R$  and the moments of resistance  $M_{Rd}$  at the limit state:

- (1) Yield limit  $y$ .
- (2) Failure limit  $u$ .

### 2.3.1. Calculation of Yield Curvature

The uniaxial bending design of the cross-section yields  $x = 187.5$  mm,  $M_{Rd,y} = 185$  kN·m,  $\varepsilon_c = 2.0\%$ , and  $\varepsilon_{s1} = 1.734\%$ . Hence, Equation (2) provides the yield curvature as follows:

$$\varphi_y = (2.0 + 1.734) \times 10^{-3} / (0.40 - 0.05) = 10.67 \times 10^{-3} / \text{m} \rightarrow R_y = 94 \text{ m}$$

The respective elastic curvature (without cracks) at the base of the column is provided by the relation as follows:

$$\varphi_e = 1/R = M_{Rd,y} / (E \cdot I)$$

According to Eurocode 2 [14], §3.1.2(3), it is  $f_{cm} = f_{ck} + 8 = 38$  MPa and  $E = 22 \times (f_{cm}/10)^{0.3} \times 10^3 = 32.8$  GPa, so  $E \cdot I = 32.8 \times (0.4 \times 0.4^3 / 12) = 70.0 \times 10^3$  kN·m<sup>2</sup>. Substituting, we get:

$$\varphi_e = 185 / (70.0 \times 10^3) = 2.64 \times 10^{-3} / \text{m} \rightarrow R_e = 379 \text{ m}$$

Therefore, it is:

$$\varphi_y / \varphi_e = 10.67 \times 10^{-3} / 2.64 \times 10^{-3} = 4.04,$$

which is very important for determining the effective stiffness of a column according to Eurocode 8 [15], §4.3.1(6, 7).

### 2.3.2. Calculation of Failure Curvature

The uniaxial bending design of the cross-section yields  $x = 156.1$  mm,  $M_{Rd,u} = 219$  kN·m,  $\varepsilon_c = 3.5\%$ , and  $\varepsilon_{s1} = 4.35\%$ . Hence, from Equation (3), the failure curvature is as follows:

$$\varphi_u = (3.5 + 4.35) \times 10^{-3} / (0.40 - 0.05) = 22.42 \times 10^{-3} / \text{m} \rightarrow R_u = 45 \text{ m}$$

Similarly to the yield state case, the elastic curvature is as follows:

$$\varphi_e = 219 / (70.0 \times 10^3) = 3.13 \times 10^{-3} / \text{m} \rightarrow R_e = 320 \text{ m}$$

Therefore, it is:

$$\varphi_u / \varphi_y = 22.42 \times 10^{-3} / 10.67 \times 10^{-3} = 2.10 \text{ and } \varphi_u / \varphi_e = 22.42 \times 10^{-3} / 3.13 \times 10^{-3} = 7.16.$$

## 3. Equilibrium of Internal and External Forces

The following relations are derived from Figure 5:

$$x = d \cdot \varepsilon_c / (\varepsilon_c + \varepsilon_s), \varepsilon_c = \varepsilon_s \cdot x / (d - x), \varepsilon_s = \varepsilon_c \cdot (d - x) / x, \varepsilon_{s2} = \varepsilon_c \cdot (x - d_2) / x \quad (4)$$

$$k_F = \alpha_{cc} \cdot f_{cd} \cdot b, F_c = k_F \cdot x \cdot \alpha, z_c = x \cdot \kappa \quad (5)$$

$$F_{s1} = A_{s1} \cdot \sigma_{s1}, F_{s2} = A_{s2} \cdot \sigma_{s2} \quad (6)$$

There are two basic equations balancing the internal forces with the external forces of a cross-section under uniaxial bending with axial force (see Figure 5):

- (a) Equilibrium equation of the forces  $F_{s1}$ ,  $F_c$ , and  $F_{s2}$  with the axial force  $N_d$

$$F_{s1} - F_c - F_{s2} = N_d \quad (7)$$

- (b) Equilibrium equation of the moments of the forces  $F_c$  and  $F_{s2}$  with the bending moment  $M_d$  in the cross-section center and the moment of axial force  $N_d$

$$M_d - N_d \cdot z_{s1} = F_c \cdot (d - z_c) + F_{s2} \cdot (d - d_2) \tag{8}$$

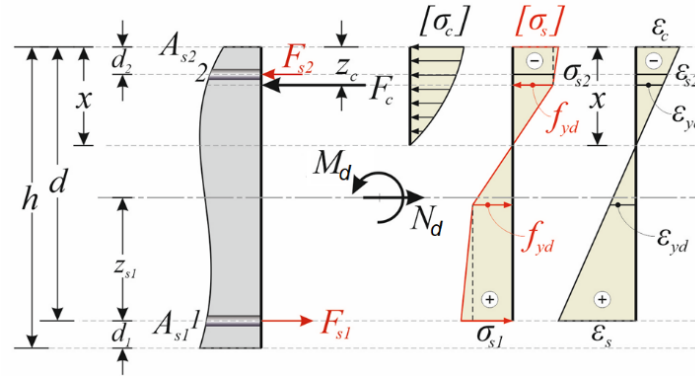


Figure 5. External and internal forces in a cross-section under uniaxial bending with axial force.

Using the Relations (4)–(6), Equations (7) and (8) transform into:

$$A_{s1} \cdot \sigma_{s1} = A_{s2} \cdot \sigma_{s2} + F_c + N_d \tag{9}$$

$$M_d = F_c \cdot (d - z_c) + A_{s2} \cdot \sigma_{s2} \cdot (d - d_2) + N_d \cdot z_{s1} \tag{10}$$

If  $\rho_1 = A_{s1}/A_c$  and  $\rho_2 = A_{s2}/A_c$ , so  $\rho_2/\rho_1 = A_{s2}/A_{s1}$  and  $A_{s2} = A_{s1} \cdot \rho_2/\rho_1$ , then Equations (9) and (10) can be written as follows:

$$A_{s1} = (F_c + N_d) / \left( \sigma_{s1} - \frac{\rho_2}{\rho_1} \cdot \sigma_{s2} \right) \tag{11}$$

$$M_d = F_c \cdot (d - z_c) + A_{s1} \cdot \frac{\rho_2}{\rho_1} \cdot \sigma_{s2} \cdot (d - d_2) + N_d \cdot z_{s1} \tag{12}$$

It is emphasized that the axial force  $N_d$  always has a given value, independent of the above relations.

The system of Equations (11) and (12) has three unknown variables in the corresponding problem, that is,  $\epsilon_c$ ,  $\epsilon_s$ , and  $A_{s1}$  or  $M_d$ . Therefore, the system solution requires additional conditions to be set, as follows:

- First condition: the reinforcement ratio  $\rho_2/\rho_1$  is provided.
- Second condition: either  $\epsilon_c$  or  $\epsilon_s$  should be in the limit state.

These two conditions, under certain assumptions, can replace the third equation. Nevertheless, the solution is rather difficult, especially in the failure state, due to numerous and complex combinations. The difficulty could be removed by using the trial solution method. However, this process would require the determination of the solution boundaries, which is also a quite complex problem.

#### 4. Solution Regions in the Yield Limit State

The regions comprising possible solutions in the yield limit state are presented in Figure 6.

Let  $\rho_2/\rho_1$  be the ratio of the compressive to the tensile reinforcement. For any given value of the ratio  $\rho_2/\rho_1$ , there is a characteristic case having compression zone depth  $x_{01}$  (see Figure 6), where the denominator of Equation (11) becomes zero. That is

$$\sigma_{s1} - \frac{\rho_2}{\rho_1} \cdot \sigma_{s2} = 0 \rightarrow \overbrace{E_s \cdot \epsilon_{s1}}^{\sigma_{s1}} - \frac{\rho_2}{\rho_1} \cdot \overbrace{E_s \cdot \epsilon_{s2}}^{\sigma_{s2}} = 0 \rightarrow \epsilon_{s1} = \frac{\rho_2}{\rho_1} \cdot \epsilon_{s2}$$

Taking into account Equation (4), the above relation can be written as

$$\overbrace{\varepsilon_c \cdot (d - x_{01}) / x_{01}}^{\varepsilon_{s1}} = \frac{\rho_2}{\rho_1} \cdot \overbrace{\varepsilon_c \cdot (x_{01} - d_2) / x_{01}}^{\varepsilon_{s2}} \rightarrow x_{01} = \left( d + \frac{\rho_2}{\rho_1} \cdot d_2 \right) / \left( 1 + \frac{\rho_2}{\rho_1} \right) \quad (13)$$

Thus, at location 01, corresponding to compression zone depth  $x_{01}$  provided by Equation (13), both tensile reinforcement  $A_{s1}$  and bending moment  $M_d$  will be infinite (see Equations (11) and (12)). Let us name this location existing in the yield limit state “Asymptotic Location”.

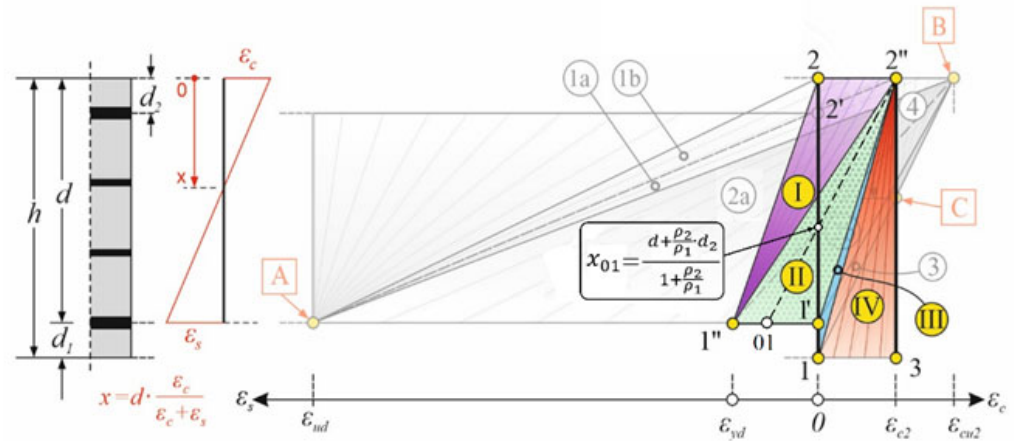


Figure 6. Permissible strain distributions in the yield limit state.

### 5. Solution Regions in the Failure Limit State

The regions comprising possible solutions in the failure limit state are presented in Figure 7. Region 1, where the steel reaches its failure limit [A], and region 2, where the concrete reaches its failure limit [B], are divided to subregions 1a, 1b and 2a, 2b respectively. Along the boundaries 2''A and 1''B, both  $M_d$  and  $A_{s1}$  tend to infinite values.

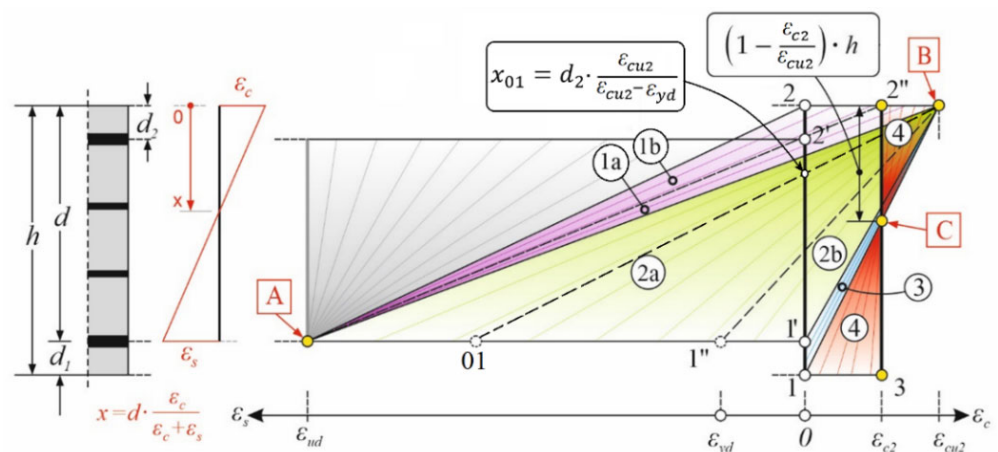


Figure 7. Permissible strain distributions in the failure limit state.

For  $\rho_2/\rho_1 = 1$ , the denominator of Equation (11) is written as  $d\sigma = \sigma_{s1} - \sigma_{s2}$ .

By observing the strain distributions in Figure 7, the following conclusions can be drawn:

- (1) The boundary 1''B of the subregions 2a and 2b, has  $\varepsilon_{s1} = \varepsilon_{yd} \rightarrow \sigma_{s1} = f_{yd}$  and  $\varepsilon_c = \varepsilon_{cu2}$ . Since it is usually  $\varepsilon_{s2} \geq \varepsilon_{yd} \rightarrow \sigma_{s2} = f_{yd}$ , we have  $d\sigma = \sigma_{s1} - \sigma_{s2} = f_{yd} - f_{yd} = 0$ .
- (2) To the left of location 1''B will continue to be  $d\sigma = 0$  until the specific location 01 with  $\varepsilon_{s1} = \varepsilon_{s2}$ .

From the last of Equations (4), for  $\varepsilon_{s2} = \varepsilon_{yd}$  and  $\varepsilon_c = \varepsilon_{cu2}$ , the compression zone depth at location 01 is as follows:

$$\varepsilon_{yd} = \varepsilon_{cu2} \cdot (x_{01} - d_2) / x_{01} \rightarrow x_{01} = d_2 \cdot \varepsilon_{cu2} / (\varepsilon_{cu2} - \varepsilon_{yd}) \quad (14)$$

Thus, for the subregion extended between locations 1''B and 01, corresponding to compression zone depths  $x_{01}$  provided by Equation (14), both the bending moment  $M_d$  and the tensile reinforcement  $A_{s1}$  will be infinite (see Equations (11) and (12)). Let us name this region existing in the failure limit state for  $\rho_2/\rho_1 = 1$  "Asymptotic Region". Notice that this asymptotic region is independent of the concrete class.

## 6. Application: The "Typical Rectangular Section" in Limit States

Consider a structural element made of C30/37 concrete and B500 steel with a 300 mm  $\times$  550 mm rectangular cross-section, as shown in Figure 8.

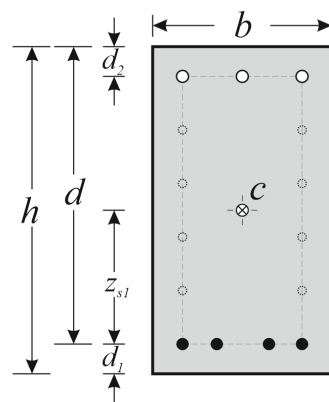


Figure 8. A typical rectangular section.

Provided:

$$b = 300 \text{ mm}, h = 550 \text{ mm}, d_2 = 50 \text{ mm}, d_1 = 50 \text{ mm},$$

$$f_{ck} = 30 \text{ MPa}, \gamma_c = 1.50, a_{cc} = 0.85, \varepsilon_{c2} = 2.0\text{‰}, \varepsilon_{cu2} = 3.5\text{‰},$$

$$f_{yk} = 500 \text{ MPa}, \gamma_s = 1.15, E_s = 200 \text{ GPa (for steel grades B500a,b,c)}$$

Derived:

$$d = h - d_1 = 500 \text{ mm}, z_{s1} = h/2 - d_1 = 0.225 \text{ m}$$

$$f_{cd} = f_{ck} / \gamma_c = 20.0 \text{ MPa}, k_F = a_{cc} \cdot b \cdot f_{cd} = 0.85 \cdot 0.30 \cdot 20.0 \cdot 10^3 = 5100 \text{ kN/m},$$

$$f_{yd} = f_{yk} / \gamma_s = 500 / 1.15 = 434.78 \text{ MPa}, \varepsilon_{yd} = f_{yd} / E_s = 434.78 / (200 \times 10^3) = 2.174\text{‰}$$

For  $\varepsilon_c = \varepsilon_{c2} = 2\text{‰}$ , it is  $\alpha = 0.6667$  and  $\kappa = 0.375$ , while for  $\varepsilon_c = \varepsilon_{cu2} = 3.5\text{‰}$ , it is  $\alpha = 0.8095$  and  $\kappa = 0.416$ .

For B500c steel grade,  $\varepsilon_{ud} = 20\text{‰}$  with  $K = 1.0$  is used in the simplified stress–strain diagram, while  $\varepsilon_{ud} = 67.5\text{‰}$  is used with  $K = 1.15$  in the exact stress–strain diagram.

### 6.1. Yield Limit State

Using the regions for the yield limit state presented in Figure 6, we form Figure 9 for the "typical rectangular cross-section", where the strain-based region boundaries and the corresponding compression zones are clearly illustrated. We define the origin of the compression zone as the outermost upper fiber of the cross-section, while  $x_{ij}$  represents the compression zone depth corresponding to the location 'ij'. For practical representation reasons, we consider the cross-section to lie horizontally.

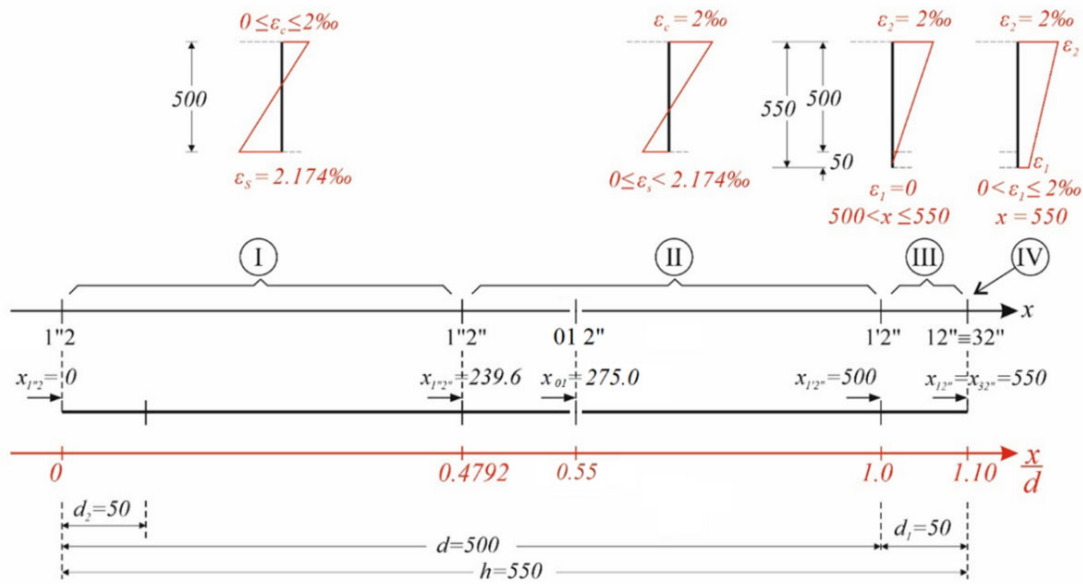


**Figure 9.** Strain-based region boundaries and corresponding compression zones in the yield limit state for the “typical rectangular section”.

### 6.1.1. Strain and Curvature Diagrams in the Yield Limit State

The diagrams of strain  $\epsilon_c$ ,  $\epsilon_s$  and the corresponding yield curvatures  $\varphi_y$  are shown in Figure 10. These values are independent of the axial force  $N_d$  and the reinforcement ratio  $\rho_2/\rho_1$ .

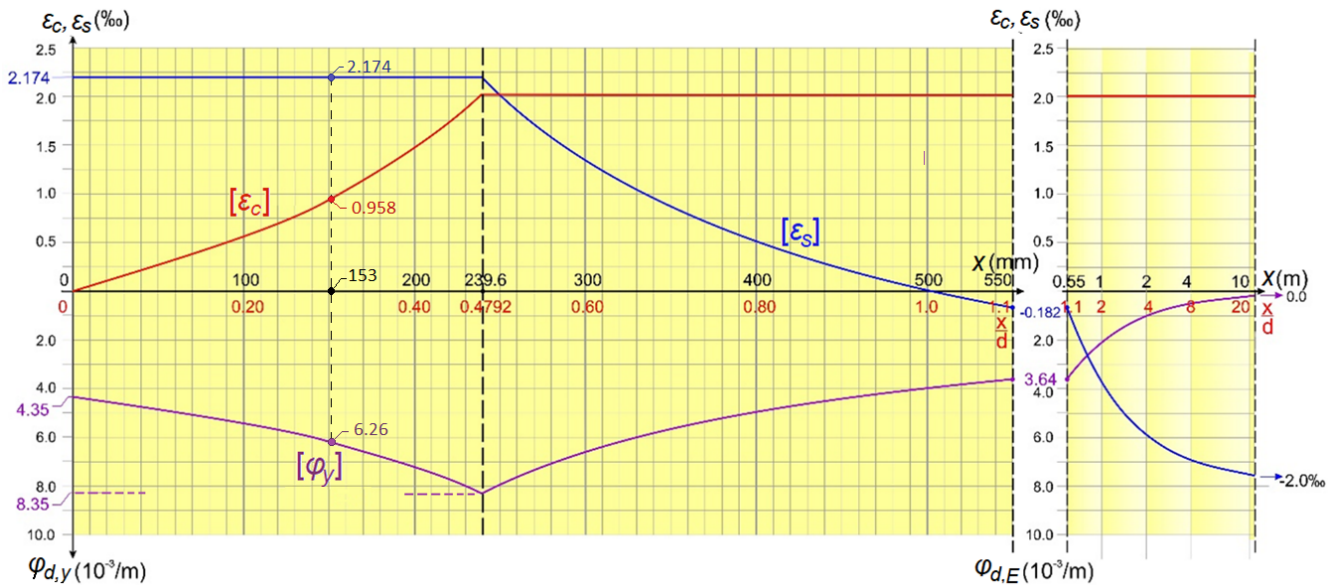


**Figure 10.** Strain diagrams and corresponding yield curvatures for the “typical rectangular section”.

The compression zone depth is presented on the diagrams in millimeters up to a depth of  $h = 550$  mm, and thereafter in meters on a logarithmic scale. In practice, the values of  $A_{s1}$  and  $M_d$  are required in each characteristic case of the cross-section with respect to  $x$ . These values, as obtained from Equations (11) and (12), depend on both the reinforcement ratio  $\rho_2/\rho_1$  and the axial force  $N_d$ .

### 6.1.2. Asymptotic Location in Yield Limit State for $\rho_2/\rho_1 = 1$

For  $\rho_2/\rho_1 = 1$ , Equation (13) yields:

$$x_{01} = (500 + 1 \times 50)/(1 + 1) = 275 \text{ mm and } (d - x_{01})/x_{01} = 0.818.$$

Since the concrete reaches its critical value in this case (i.e.,  $\varepsilon_c = \varepsilon_{c2} = 2.0\%$ ), Equation (4) yield a tensile strain value for steel  $\varepsilon_{s1} = 2.0\% \times 0.818 = 1.636\%$ . On the other hand, for  $\varepsilon_c = \varepsilon_{c2} = 2\%$ , it is  $\alpha = 0.6667$  and  $\kappa = 0.375$  (see Section 6). Consequently, from Equation (5) the compressive force  $F_c$  received by the concrete is  $F_c = k_F \cdot x_{01} \cdot \alpha = 5100 \times 0.275 \times 0.6667 = 935.0 \text{ kN}$ .

### 6.1.3. Solution Nomogram in Yield Limit State for $\rho_2/\rho_1 = 1$

The method of reinforcement with  $A_{s2} = A_{s1}$  (i.e.,  $\rho_2/\rho_1 = 1$ ) is used in cases where significant axial forces are exerted mainly on columns and/or in cases of beams with special anti-seismic requirements that entail high plasticity requirements [16].

Figure 11 presents a solution nomogram in the yield limit state for  $\rho_2/\rho_1 = 1$ , in the form of paired diagrams ( $M_d, A_{s1}$ ) corresponding to different compression zone depths  $x$  and axial forces  $N_d$ . The asymptotic location here stands for  $x_{01} = 275.0 \text{ mm}$ , and therefore, region II is divided into two subregions (see Figure 9). For this case, it is  $\varepsilon_c = 2.0\%$  and  $F_c = 935.0 \text{ kN}$  (see results in Section 6.1.2).

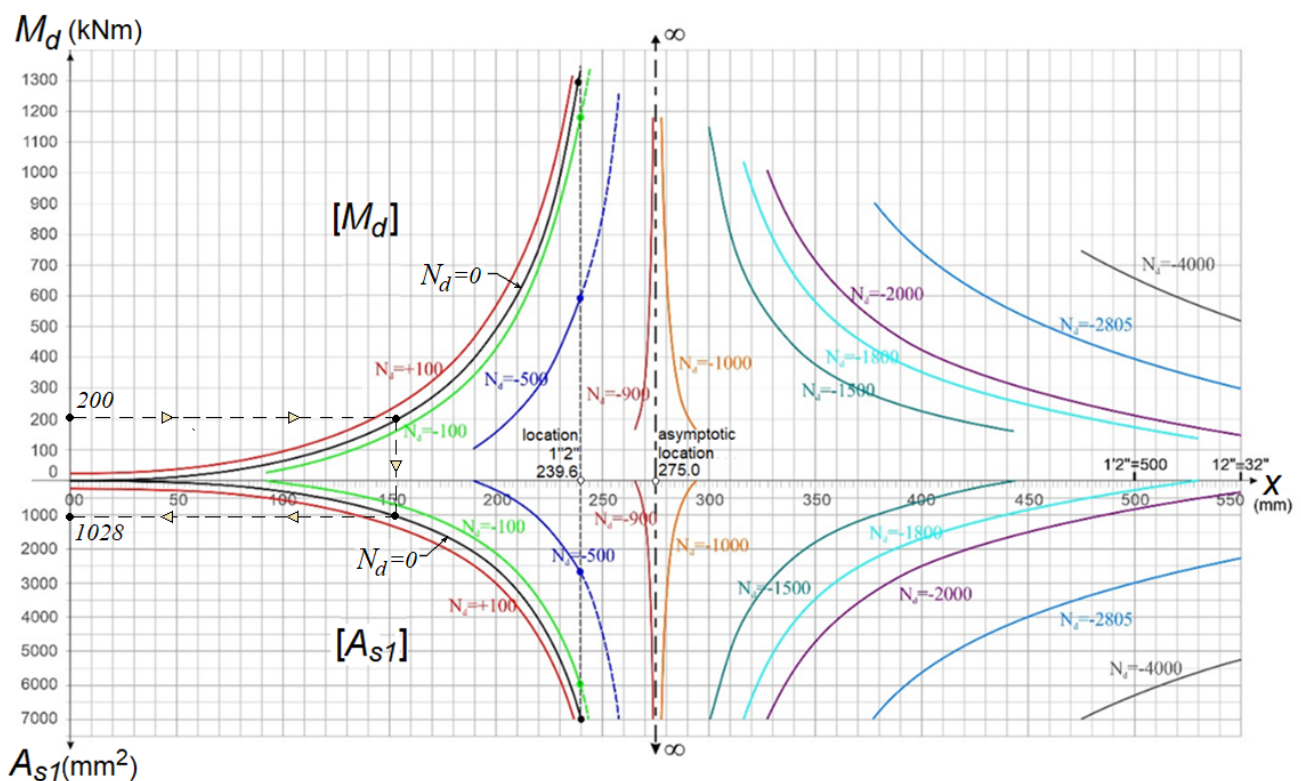


**Figure 11.** Paired diagrams ( $M_d, A_{s1}$ ) corresponding to compression zone depths  $x$  and axial forces  $N_d$  in yield limit state for the “typical rectangular section” and  $\rho_2/\rho_1 = 1$ .

At each position  $x$ , there is a specific pair ( $A_{s1}, M_d$ ) calculated from Equations (11) and (12). For example, for bending moment  $M_d = 200 \text{ kN}\cdot\text{m}$  and axial force  $N_d = 0 \text{ kN}$ , the steel reaches the yield state first, so the required tensile reinforcement is  $A_{s1} = 1028 \text{ mm}^2$  (see Figure 11). The respective compression zone depth is found to be  $x = 153.0 \text{ mm}$ , resulting in strains  $\varepsilon_c = 0.958\%$  and  $\varepsilon_s = 2.174\%$ , clearly indicating that the steel has reached its yield

point (see Figure 10). Then, Equation (2) provides the yield curvature (also presented in Figure 10).

$$\varphi_y = (0.958 + 2.174) \times 10^{-3} / (0.55 - 0.05) = 6.26 \times 10^{-3} / \text{m}.$$

### 6.2. Failure Limit State

Using the regions for the failure limit state presented in Figure 7, we form Figure 12 for the “typical rectangular cross-section” where the strain-based region boundaries and the corresponding compression zones are illustrated. In any algorithmic process adopted, the region boundaries should be first determined, because the upper and lower bounds of  $x$  and the corresponding values of the non-critical strain of the steel or concrete are needed. In the case of an accurate stress–strain diagram of the steel, for example, for  $\epsilon_{ud} = 67.5\%$  and  $K = 1.15$ , the region boundaries A2” and AB change significantly, but the calculation process remains the same. Furthermore, such differences in reinforcement design values are trivial in practice.

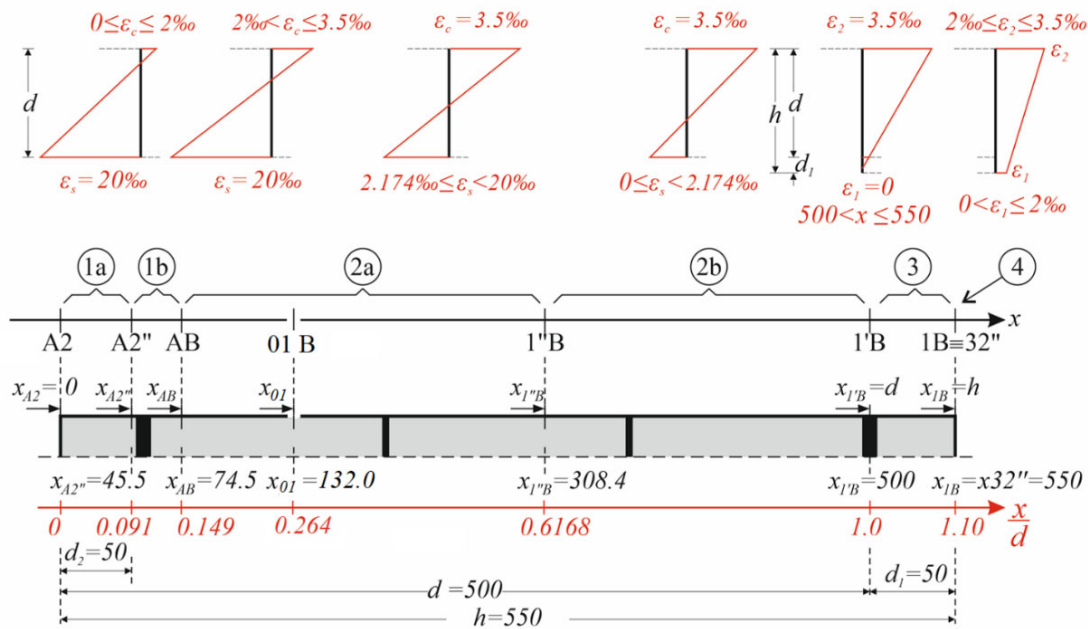


**Figure 12.** Strain-based region boundaries and corresponding compression zones in the failure limit state for the “typical rectangular section”.

#### 6.2.1. Strain and Curvature Diagrams in the Failure Limit State

The diagrams of strain  $\epsilon_c$ ,  $\epsilon_s$  and the corresponding failure curvatures  $\varphi_u$  state are presented in Figure 13. For comparison reasons, the corresponding yield curvatures  $\varphi_y$  are also shown. Notice that all values are independent of the axial force  $N_d$  and the reinforcement ratio  $\rho_2/\rho_1$ . The compression zone depth  $x$  is given in millimeters up to the total depth of  $h = 550$  mm, and from there on, in meters on a logarithmic scale. In practice, the values of  $A_{s1}$  and  $M_d$  are required at each characteristic location of the cross-section with respect to  $x$ . These values, obtained from Equations (11) and (12), depend on both the reinforcement ratio  $\rho_2/\rho_1$  and the axial force  $N_d$ .

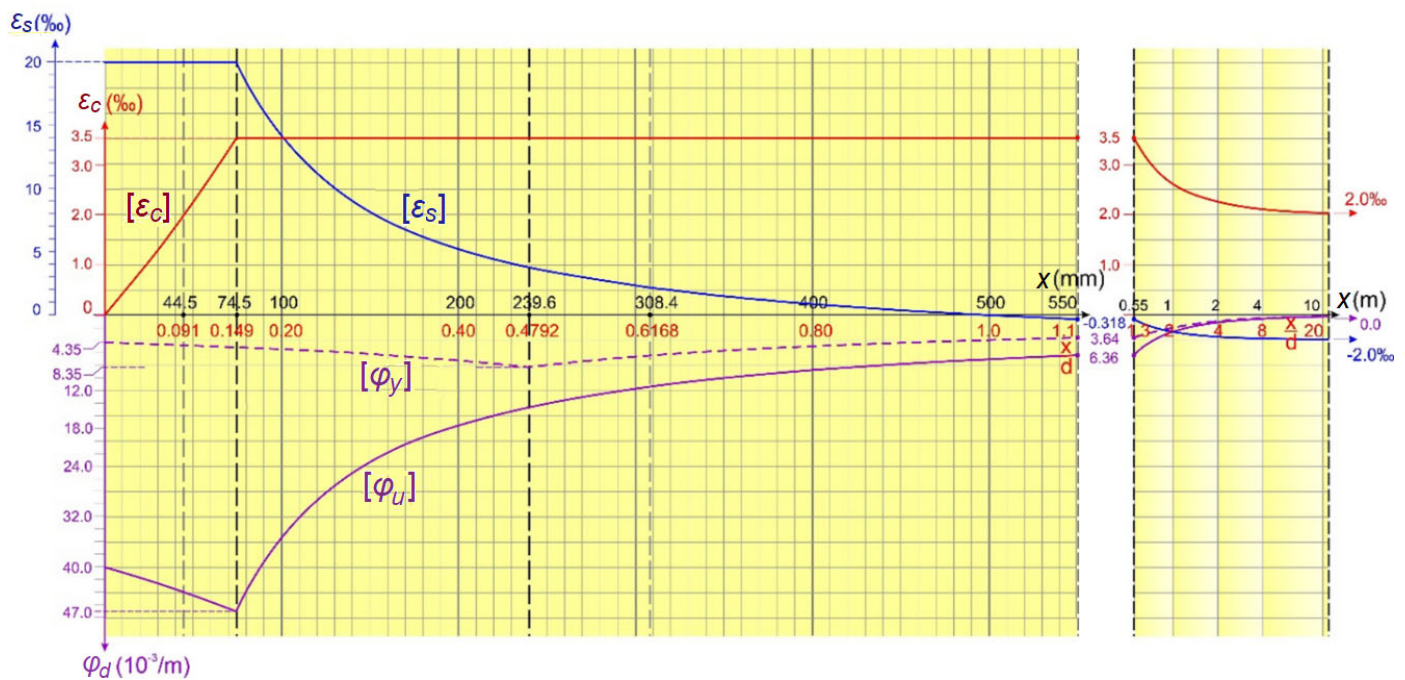


**Figure 13.** Strain diagrams and corresponding curvatures in the failure limit state for the “typical rectangular section”.

### 6.2.2. Asymptotic Region in Failure Limit State for $\rho_2/\rho_1 = 1$

Equation (14) gives  $x_{01} = 50 \times 3.5 / (3.50 - 2.174) = 132.0$  mm, while Equation (5) give the force  $F_c = 5100 \times 0.132 \times 0.8095 = 544.9$  kN received by the concrete at the location 01.

Equation (4) give  $x_{1''B} = 500 \times 3.5 / (3.5 + 2.174) = 308.4$  mm, while Equation (5) give the force  $F_c = 5100 \times 0.3084 \times 0.8095 = 1273.2$  kN received by the concrete at the location 1''B.

Thus, Equation (11) maintains a zero denominator throughout the interval between  $x_{01} = 132.0$  mm and  $x_{1''B} = 308.4$  mm.

### 6.2.3. Solution Nomogram in Failure Limit State for $\rho_2/\rho_1 = 1$

Figure 14 presents a solution nomogram for  $\rho_2/\rho_1 = 1$ , in the form of paired diagrams ( $M_d, A_{s1}$ ) corresponding to different compression zone depths  $x$  and axial forces  $N_d$ . At each position  $x$ , there is a specific pair ( $A_{s1}, M_{sd}$ ) calculated from Equations (11) and (12). The diagram comprises the areas of dominant bending on the left and the areas of dominant compression on the far right. A multiple solution area is also apparent in the middle, theoretically extending to infinity. It should be pointed out that in our case, with  $\rho_2/\rho_1 = 1$ , there are two asymptotic boundary locations (in the sense of zeroing the denominator of Equation (11)), that is, 01 and 1''B, as determined in Section 6.2.2. Consequently, region 2a is divided into two subregions (AB, 01) and (01, 1''B) (see Figures 7 and 12).

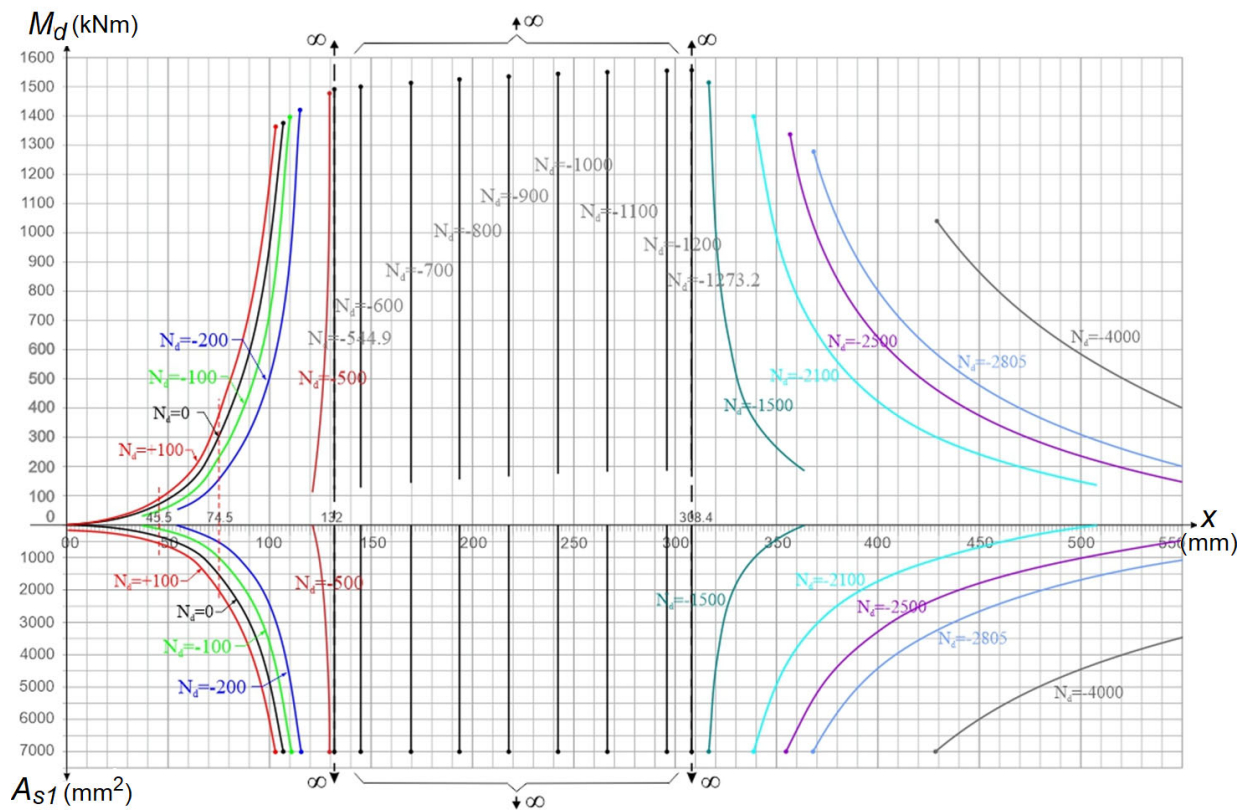


**Figure 14.** Paired diagrams ( $M_d, A_{s1}$ ) corresponding to compression zones  $x$  and axial forces  $N_d$  in the failure limits state for the “typical rectangular section” and  $\rho_2/\rho_1 = 1$ .

6.2.4. Indeterminacy or Multiple Solution Region in Failure Limit State

This region extends between the two asymptotic locations 01 and 1''B, corresponding to compression zone depths  $x_{01} = 132$  mm and  $x_{1''B} = 308.4$  mm, respectively (see Figure 14).

By relating those to the respective forces, we can say that a cross-section is in the indeterminacy region when stressed by axial forces of  $544.9 \text{ kN} \leq N_d \leq 1273.2 \text{ kN}$  (see results in Section 6.2.2).

In this region, it is  $\sigma_{s1} = \sigma_{s2}$ . Thus, Equation (11) gives indeterminacy  $A_{s1} = \infty$  for  $F_c \neq -N_d$  and an infinite number of solutions for  $F_c = -N_d$ . For each  $N_d$  in the region, there is a certain  $x$  that gives  $F_c = -N_d$ . This location has  $x = F_c / \alpha_{cc} \cdot f_{cd} \cdot b \cdot \alpha$ , and the force  $F_c$  is exerted at the position  $z_c = x \cdot \kappa$  (where  $\alpha = 0.8095$  and  $\kappa = 0.416$  because  $\epsilon_c = \epsilon_{cu2} = 3.5\%$ —see values in Section 6). Furthermore, the tensile strain is  $\epsilon_{s1} = \epsilon_c \cdot (d - x) / x$ , while the force is  $F_{s2} = A_{s2} \cdot \sigma_{s2} = A_{s1} \cdot f_{yd}$ .

Since  $F_c = -N_d, \rho_2/\rho_1 = 1$ , and  $\sigma_{s2} = \sigma_{s1} = f_{yd}$ , Equation (12) yields:

$$M_d = A_{s1} \cdot f_{yd} \cdot (d - d_2) - N_d \cdot (d - z_c - z_{s1}) \tag{15}$$

Notice that Equation (15) directly relates  $A_{s1}$  to  $M_d$ . So, when  $M_d$  is given in a problem,  $A_{s1}$  is uniquely calculated, while when  $A_{s1}$  is given,  $M_d$  is uniquely calculated.

Remark: In the multiple solution region, all pairs ( $M_d, A_{s1}$ ) having the same  $N_d$  correspond to the same  $x$ , implying the same strains  $\epsilon_{s1}$  and  $\epsilon_c$  and, hence, constant failure curvatures  $\varphi_u$ .

6.2.5. Application in Failure Limit State for  $\rho_2/\rho_1 = 1$  and  $N_d = -1000$  kN

It is  $x = 1000 / (0.85 \times 20 \times 10^3 \times 0.30 \times 0.8095) = 0.2422$  m,  $z_c = 0.2422 \times 0.416 = 0.101$  m,  $\epsilon_{s1} = 3.5 \times (0.50 - 0.2422) / 0.2422 = 3.73\%$ ,  $\epsilon_c = 3.5\%$ , and  $\varphi_u = (3.5 + 3.73) / 0.50 = 14.46\%$  / m.

For  $A_{s1} = A_{s2} = 0$  (when reinforcement is barely required), Equation (15) yields  $M_d = 0 + 1000 \times (0.50 - 0.101 - 0.225) = 174$  kN·m. That is, for axial force  $N_d = -1000$  kN and moment  $M_d \leq 174$  kN·m, no reinforcement is required.

For  $A_{s1} = A_{s2} = 7000$  mm<sup>2</sup> (selection of maximum reinforcement value  $A_{s1}$  in Figure 14), Equation (15) yields  $M_d = 7000 \times 10^{-6} \times 434.78 \times 10^3 \times (0.50 - 0.05) + 1000 \times (0.50 - 0.101 - 0.225) = 1544$  kN·m.

For  $M_d = 800$  kN·m, inverted Equation (15) yields  $A_{s1} = [800 - 1000 \times (0.50 - 0.101 - 0.225)] / [434.78 \times 10^3 \times (0.50 - 0.05)] = 3.200 \times 10^{-3}$  m<sup>2</sup> = 3200 mm<sup>2</sup>. Hence, the solution is determined as a pair (800, 3200) from the infinite number of pairs of specific solutions on the line  $N_d = -1000$  kN.

## 7. Conclusions

- The influence of cracking on the curvature of RC elements is significant in relation to the corresponding elastic curvature, even in the yield state, so the corresponding yield stiffness is significantly smaller than the elastic stiffness.
- For specific flexural reinforcement, the yield curvature is much smaller than the failure curvature, while the yield moment of resistance is of the same order of magnitude as the failure moment of resistance.
- During the bending design of a cross-section in the failure limit state, there is an extended region of compressive axial forces where the curvature is practically constant regardless of the acting moment. Then, for any given axial force, the necessary flexural reinforcement is derived from the acting moment based on a first-order equation.
- It is proposed that the design process should take place in the following order:
  - (a) Calculate reinforcement in the failure state.
  - (b) Choose and apply reinforcement.
  - (c) Calculate failure curvatures  $\varphi_u$ , yield curvatures  $\varphi_y$ , and elastic curvatures  $\varphi_e$ .
  - (d) Estimate curvature ductilities from the ratios  $\varphi_u/\varphi_y$  and/or  $\varphi_u/\varphi_e$ .
  - (e) Determine effective stiffness and resolve.

**Author Contributions:** Conceptualization, A.K.; Data curation, J.B.; Methodology, A.K.; Resources, J.B.; Software, J.B.; Formal analysis, A.K.; Validation, J.B.; Investigation, A.K.; Writing—original draft, A.K.; Writing—review & editing, J.B.; Visualization, A.K. All authors have read and agreed to the published version of the manuscript.

**Funding:** This research received no external funding.

**Data Availability Statement:** The raw data supporting the conclusions of this article will be made available by the authors on request.

**Conflicts of Interest:** Author Apostolos Konstantinidis is the director of the company BuildingHow PC. The remaining author declares that the research was conducted in the absence of any commercial or financial relationships that could be construed as a potential conflict of interest.

## Nomenclature

The following symbols are employed in this paper:

|               |   |
|---------------|---|
| $A_s$         | total reinforcement   |
| $A_{s1}$      | tensile reinforcement                                       |
| $A_{s2}$      | compressive reinforcement                                   |
| $\alpha_{cc}$ | long-term effects factor                                    |
| $b$           | beam width  |
| $c$           | ratio of compressive reinforcement to tensile reinforcement |
| $d$           | beam effective depth  |
| $d_1$         | tensile reinforcement cover                                 |
| $d_2$         | compressive reinforcement cover                             |
| $E$           | concrete modulus of elasticity                              |
| $E_s$         | steel modulus of elasticity                                 |

|                  |  |
|------------------|--|
| $F_c$            | concrete compressive force   |
| $F_{s1}$         | tensile reinforcement force  |
| $F_{s2}$         | compressive reinforcement force  |
| $f_{ck}$         | concrete compressive strength  |
| $f_{cm}$         | concrete mean compressive strength   |
| $f_{yk}$         | steel yield strength   |
| $f_{cd}$         | concrete design strength   |
| $f_{yd}$         | steel design strength  |
| $h$              | beam height  |
| $I$              | cross-section moment of inertia  |
| $K$              | strain hardening coefficient (ductility property)                                  |
| $k_F$            | concrete compressive force coefficient   |
| $M_d$            | bending moment acting in the cross-section center                                  |
| $M_{sd}$         | bending moment acting in the tensile reinforcement position                        |
| $N_d$            | axial force acting in the cross-section center                                     |
| $R_e$            | radius of elastic curvature  |
| $R_y$            | radius of yield curvature  |
| $R_u$            | radius of failure curvature  |
| $x$              | compressive zone depth distance of the outermost upper fiber from the neutral axis |
| $x_{ij}$         | compressive zone depth corresponding to the "ij" location                          |
| $x_{01}$         | compressive zone depth corresponding to the asymptotic location                    |
| $z_c$            | distance of the outermost upper fiber from the concrete compression center         |
| $z_{s1}$         | distance of the tensile reinforcement position from the cross-section center       |
| $\alpha$         | distribution factor of concrete compressive force                                  |
| $\gamma_c$       | concrete safety factor   |
| $\gamma_s$       | steel safety factor  |
| $\delta_1$       | yield state displacement due to shear  |
| $\delta_2$       | yield state displacement due to bending  |
| $\epsilon_c$     | concrete strain  |
| $\epsilon_{c2}$  | concrete yield strain  |
| $\epsilon_{cu2}$ | concrete ultimate strain   |
| $\epsilon_s$     | steel strain   |
| $\epsilon_{s1}$  | tensile reinforcement strain   |
| $\epsilon_{s2}$  | compressive reinforcement strain   |
| $\epsilon_{su}$  | steel ultimate strain  |
| $\epsilon_{ud}$  | steel design ultimate strain   |
| $\kappa$         | position factor of concrete compressive force                                      |
| $\rho_1$         | tensile reinforcement percentage   |
| $\rho_2$         | compressive reinforcement percentage   |
| $\sigma_{s1}$    | tensile reinforcement stress   |
| $\sigma_{s2}$    | compressive reinforcement stress   |
| $\varphi_e$      | elastic curvature  |
| $\varphi_y$      | yield curvature  |
| $\varphi_u$      | failure curvature  |

## References

- Chen, C.C.; Hsu, S.M. Formulas for Curvature Ductility Design of Doubly Reinforced Concrete Beams. *J. Mech.* **2004**, *20*, 257–265. [[CrossRef](#)]
- Hernández-Montes, E.; Aschheim, M.; Gil-Martín, L.M. Impact of Optimal Longitudinal Reinforcement on the Curvature Ductility Capacity of Reinforced Concrete Column Sections. *Mag. Concr. Res.* **2004**, *56*, 499–512. [[CrossRef](#)]
- Chandrasekaran, S.; Nunziante, L.; Serino, G.; Carannante, F. Curvature Ductility of RC Sections Based on Eurocode: Analytical Procedure. *KSCE J. Civ. Eng.* **2010**, *15*, 131–144. [[CrossRef](#)]
- Arslan, G.; Cihanli, E. Curvature Ductility Prediction of Reinforced High-strength Concrete Beam Sections. *J. Civ. Eng. Manag.* **2010**, *16*, 462–470. [[CrossRef](#)]
- Lee, H.-J. Predictions of Curvature Ductility Factor of Doubly Reinforced Concrete Beams with High Strength Materials. *Comput. Concr.* **2013**, *12*, 831–850. [[CrossRef](#)]
- Laterza, M.; D'Amato, M.; Thanthirige, A.P.; Braga, F.; Gigliotti, R. Comparisons of Codal Detailing Rules for Curvature Ductility and Numerical Investigations. *Open Constr. Build. Technol. J.* **2014**, *8*, 132–141. [[CrossRef](#)]

7. Zhou, J.; He, F.; Liu, T. Curvature Ductility of Columns and Structural Displacement Ductility in RC Frame Structures Subjected to Ground Motions. *Soil. Dyn. Earthq. Eng.* **2014**, *63*, 174–183. [[CrossRef](#)]
8. Baji, H.; Ronagh, H.R. Probabilistic Models for Curvature Ductility and Moment Redistribution of RC Beams. *Comput. Concr.* **2015**, *16*, 191–207. [[CrossRef](#)]
9. Breccolotti, M.; Materazzi, A.L.; Regnicoli, B. Curvature Ductility of Biaxially Loaded Reinforced Concrete Short Columns. *Eng. Struct.* **2019**, *200*, 109669. [[CrossRef](#)]
10. Kollerathu, J.A. Curvature Ductility of Reinforced Masonry Walls and Reinforced Concrete Walls. In *Sustainability Trends and Challenges in Civil Engineering: Select Proceedings of CTCS 2020; Lecture Notes in Civil Engineering*; Springer: Singapore, 2021; pp. 9–23. [[CrossRef](#)]
11. Foroughi, S.; Yuksel, S.B. A New Approach for Determining the Curvature Ductility of Reinforced Concrete Beams. *Slovak. J. Civ. Eng.* **2022**, *30*, 8–20. [[CrossRef](#)]
12. Karayannis, C.G. *Design and Behavior of Reinforced Concrete Structures for Seismic Actions: Chapter 8—Element Ductility*; Editions SOFIA: Sofia, Bulgaria, 2019; (In Greek). ISBN 978-960-633-005-6.
13. Konstantinides, A. *Earthquake Resistant Buildings Made of Reinforced Concrete: The Art of Construction and the Detailing According to Eurocodes*; Alta Grafico SA: Ano Liossia, Greece, 2010; Volume A, ISBN 978-960-85506-3-6.
14. *EN 1992-1-1: 2004*; Eurocode 2: Design of Concrete Structures. Part 1-1: General Rules and Rules for Buildings. British Standard Institution: London, UK, 2005.
15. *EN 1998-1: 2004*; Eurocode 8: Design of Structures for Earthquake Resistance. Part 1: General Rules, Seismic Actions and Rules for Buildings. European Committee for Standardization: Brussels, Belgium, 2005.
16. Konstantinides, A.; Bellos, J. *Earthquake Resistant Buildings Made of Reinforced Concrete: Static and Dynamic Analysis According to Eurocodes*; Alta Grafico SA: Ano Liossia, Greece, 2013; Volume B, ISBN 978-960-85506-4-3.

**Disclaimer/Publisher’s Note:** The statements, opinions and data contained in all publications are solely those of the individual author(s) and contributor(s) and not of MDPI and/or the editor(s). MDPI and/or the editor(s) disclaim responsibility for any injury to people or property resulting from any ideas, methods, instructions or products referred to in the content.